Supplementary Information

Supplementary Videos

Video 1. ATP6 transgenic mouse with paralysis of the hind limbs.

Video 2. ATP6 mouse with seizures.

Video 3. ATP6 mouse with quadriparesis and weight loss.

Video 4. ATP6 mouse with paraparesis prior to injection can move the hindquarters 3 days after intravenous mitochondria targeted AAV9-containing the wild-type ATP6 allele.

Video 5&6. Confocal microscopy of Hela cells 4h after transduction with mito-targeted AAV9, stained with AAV antibody showing colocalization with mitochondrial marker, Porin.

Supplementary Tables

Table 1 Mito-targeted AAV2/mutATP6 injection of mouse zygotes.

Injection Date (Date of Birth)	# Embryos Collected (# Donor Mice)	# Embryos Injected	# Embryos Lysed (% of Injected)	# Embryos Transferred	# Mice Born (% of Transferred)
3/25/13 (4/14/13)	298 (14)	266	38 (14.3%)	228	53 (23.2%)

Table 2 Summary of transgenic A6 mouse generations.

	F	M	Pup	Total
F0	31	22		53
F1	20	28	48	96
F2	52	34	12	98
F3	31	13		44
F4	62	50		112
F5	50	47		97
F6	6	9		15
Total	252	203	60	515

Pups died after birth less than ≤8 days.

Table 3 Summary of transgenic A6 mouse disease characteristics

Premature Death ≤6m	Premature Death ≤15m	Hunching	Paralysis	Seizure	Tumor	Weight loss	Ocular defects PERG/ERG/HE	Off balance
101/515 19.6%	167/515 32.4%	38/515 7.4%	16/515 3.1%	4/515 0.8%	36/515 7%	51/515 9.9%	35/43 81.4% F0-F2	40/68* 58.8% F0-F1

Columns 1-2: Premature death; Columns 3-7: survivors; % refers to total number of A6 mice (515; including F0-F6). Seizure numbers are likely underestimated because colonies were not under 24/7 surveillance. *Off balance included 31 F0 mice at ages 6, 9 and 12 months and 37 F1 at ages 7 and 10 months.

Table 4 Primers used for site directed mutagenesis of human m.8993T>G ATP6

Forward-ATT CAA CCA ATA GCC C**G**G GCC GTA CGC CTA ACC G

Reverse-CGG TTA GGC GTA CGG CC**G** GGG CTA TTG GGT TGA ATG

Underlined and bolded letters indicate mutated nucleotides.

Table 5 Primers for cloning of COX8 into AAV9

Forward-ATG TCC GTC CTG ACG CCG CTG CTG CTG CGG GGC TTG ACA GGC TCG GCCCGG CGG CTC CCA GTG CCG CGC GCC AAG GCT CCT GGA AAG AAG AAG

Reverse-CTT GGC GCG CGG CAC TGG GAG CCG CCG GGC CGA GCC TGT CAA GCC CCG CAG CAG CAG CGG CGT CAG GAC GGA CAT CCT AAC AGG TTC CTC AAC CAG G

Underlined letters are the COX8 fragment.

Table 6 Selected peptides identified by Mass Spectroscopy of FLAG-positive bands from one dimensional native gel.

Unique	Total	Reference	Gene Symbol	Gene Name
17	68	Q6PIE5|AT1A2_MOUSE	Atp1a2	ATPase, Na^+/K^+ transporting, alpha 2 (+) polypeptide
17	30	Q8R429|AT2A1_MOUSE	Atp2a1	ATPase sarcoplasmic/endoplasmic reticulum Ca2+ transporting 1
17	54	O55143|AT2A2_MOUSE	Atp2a2	ATPase sarcoplasmic/endoplasmic reticulum Ca2+ transporting 2
48	450	Q03265|ATPA_MOUSE	Atp5a1	ATP synthase, mitochondrial F1 complex, alpha subunit 1
46	350	P56480|ATPB_MOUSE	Atp5b	ATP synthase, mitochondrial F1 complex, beta subunit
13	69	Q9CQQ7|AT5F1_MOUSE	Atp5f1	ATP synthase, mitochondrial F0 complex, subunit B1
6	40	Q9DCX2|ATP5H_MOUSE	Atp5h	ATP synthase, mitochondrial F0 complex, subunit D
13	70	Q9DB20|ATPO_MOUSE	Atp5o	ATP synthase, mitochondrial F1 complex, subunit O
4	8	P03930|ATP8_MOUSE	Mtatp8	mitochondrially encoded ATP synthase 8
14	78	Q91VR2|ATPG_MOUSE	Atp5c1	ATP synthase, mitochondrial F1 complex, gamma polypeptide 1
3	24	Q9CPQ8|ATP5L_MOUSE	Atp5l	ATP synthase, mitochondrial F0 complex, subunit G
8	26	P51863|VA0D1_MOUSE	Atp6v0d1	ATPase V0 subunit d1
2	2	Q9DB20|ATPF_MOUSE	Atpf	ATP synthase subunit f
21	64	Q9Z1G4|VPP1_MOUSE	Atp6v0a1	ATPase V0 subunit a1
5	29	Q06185|ATP5I_MOUSE	Atp5i	ATP synthase, mitochondrial F0 complex subunit E
4	13	P97450|ATP5J_MOUSE	Atp5j	ATP synthase, mitochondrial F0 complex, subunit F
4	13	P14094|ATP1B1_MOUSE	Atp1b1	ATPase, beta 1 polypeptide

Supplementary Figures

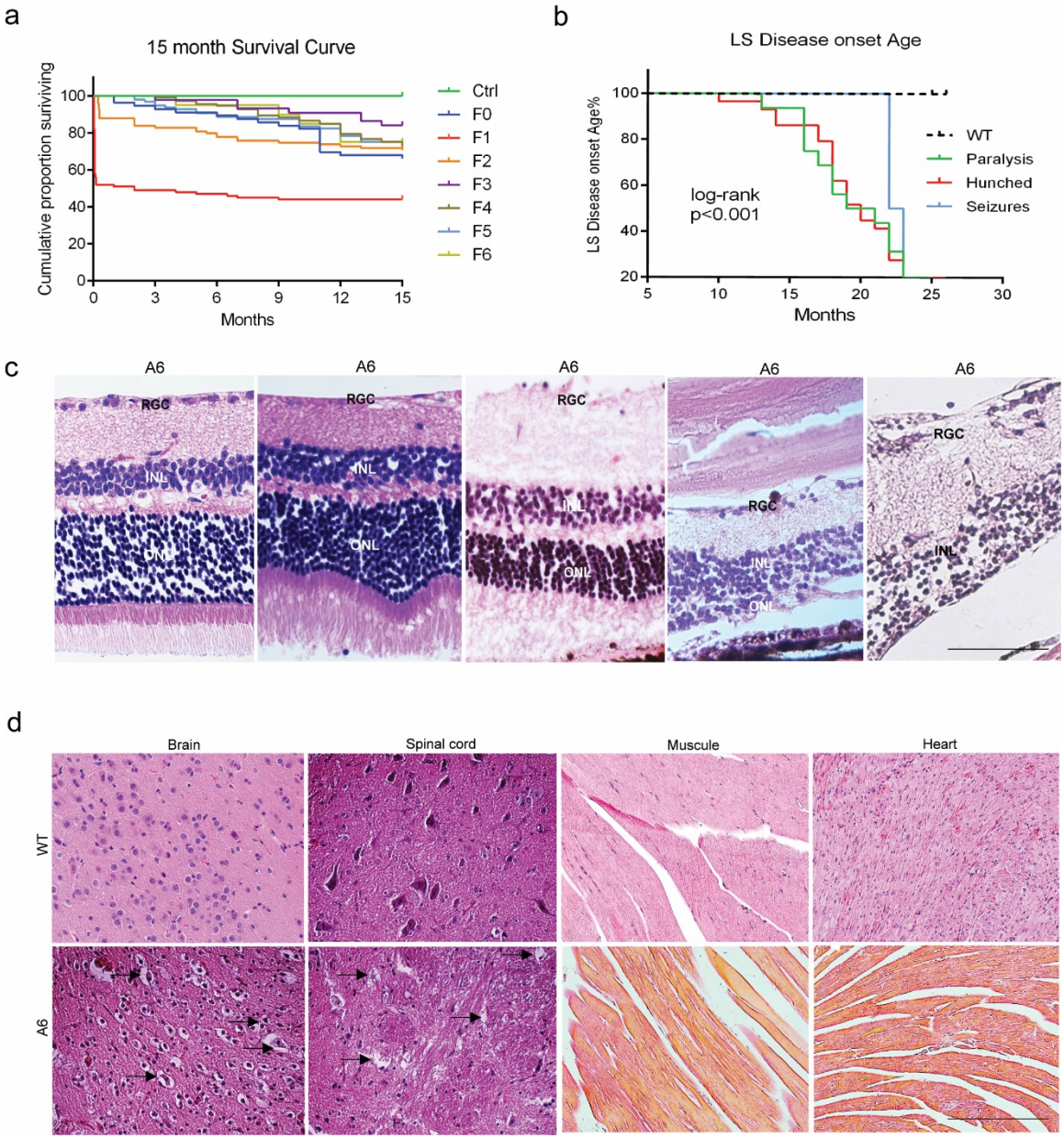

Figure 1. Human-like LS phenotypes and histopathology in A6 mice.

a. 15-month cumulative proportional survival curve for each generation of offspring (death before 15 months of age, n=167, $p<0.023$ to $p<0.0001$, log-rank test)**.**

b. Cumulative proportional Leigh syndrome disease onset including severe hind limb paralysis, hunching and seizures with age range from 10 to 26 months and generations F1 to F6.

c. Histopathology of A6 mouse eyes shows loss of retinal ganglion cells and/or outer nuclear layer cells in A6 mouse retina (scale bar: 20µm).

d. Histopathology of A6 mouse brain, spinal cord, muscle, and heart (bottom panel) compared with wild types (scale bar: 20μm).

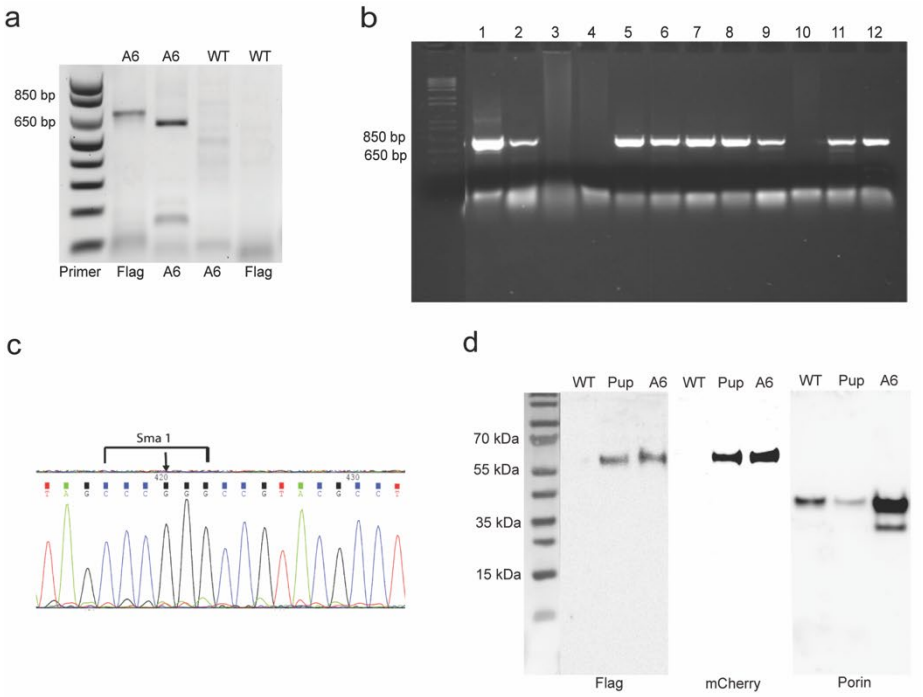
a
A6 A6 WT WT
850 bp
650 bp
Primer Flag A6 A6 Flag
b
1 2 3 4 5 6 7 8 9 10 11 12
850 bp
650 bp
c
Sma 1
d
WT Pup A6 WT Pup A6 WT Pup A6
70 kDa
55 kDa
35 kDa
15 kDa
Flag
mCherry
Porin

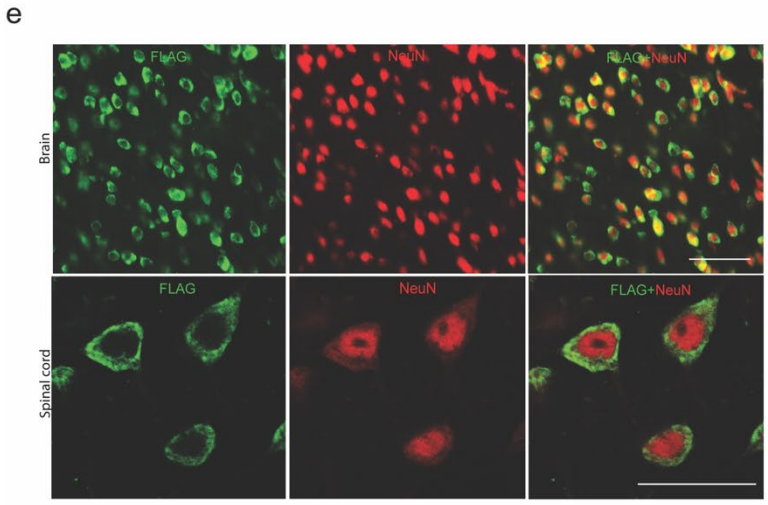
e
Brain
FLAG
NeuN
FLAG+NeuN
Spinal cord
FLAG
NeuN
FLAG+NeuN

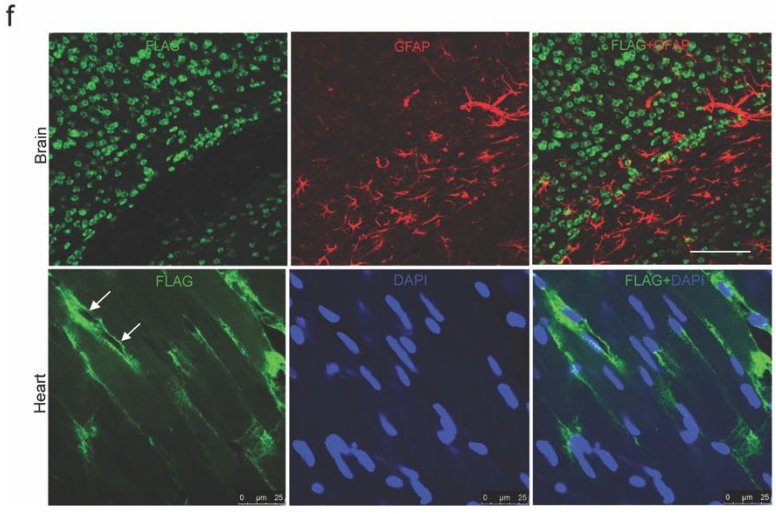
f
Brain
FLAG
GFAP
FLAG+GFAP
Heart
FLAG
DAPI
FLAG+DAPI

Figure 2. Mutant human m.8993T>G ATP6 expression in A6 mice.

a. Agarose gel electrophoresis of human *ATP6* DNA fragments amplified by human *ATP6* and FLAG primers respectively from liver mitochondria of founder mice. (M: DNA marker; A6: 695bp band amplified by human ATP6 and FLAG primers. The 604bp band was amplified by human ATP6 primers). No bands are evident in wild-type (WT) mice.

b. DNA agarose gel of mutant human ATP6 gene amplified from A6 mouse brain and/or spinal cord mitochondria with specific human ATP6 primers (lane 1-4: F2, F4, F5, F6 A6 mouse brain mtDNA; lane 5-8: F3, F5, F0, F0 brain mtDNA; lane 8-12: F0, F0, F2, F2 mouse spinal cord mtDNA).

c. ABI chromatogram of DNA fragments amplified from paraplegic murine spinal cord with mutant human m.8993 T>G ATP6 (arrow) introducing a Sma I site (CCC/GGG).

d. SDS-PAGE western blot analysis shows that expression of mutant human ATP6 in early death pup brain was greater than A6 mouse brain stained by FLAG and mCherry antibodies respectively in contrast to wild type mouse (porin as a loading control).

e. Immunostaining shows mutant human ATP6 fused to FLAG displayed around the neuron nucleus (NeuN: Neuron cell nuclear marker) in A6 mouse brain (upper panel) and spinal cord (bottom panel, scale bar: 25μm).

f. Immunofluorescence images show mutant human ATP6 fused Flag in an A6 brain display a perinuclear pattern within the neurons that is absent in glial cells (upper panel, scale bar: 25μm). Images in the bottom panel show perinuclear pattern of mutant human ATP6 fused FLAG expressed in A6 mouse hearts (scale bar: 25μm).

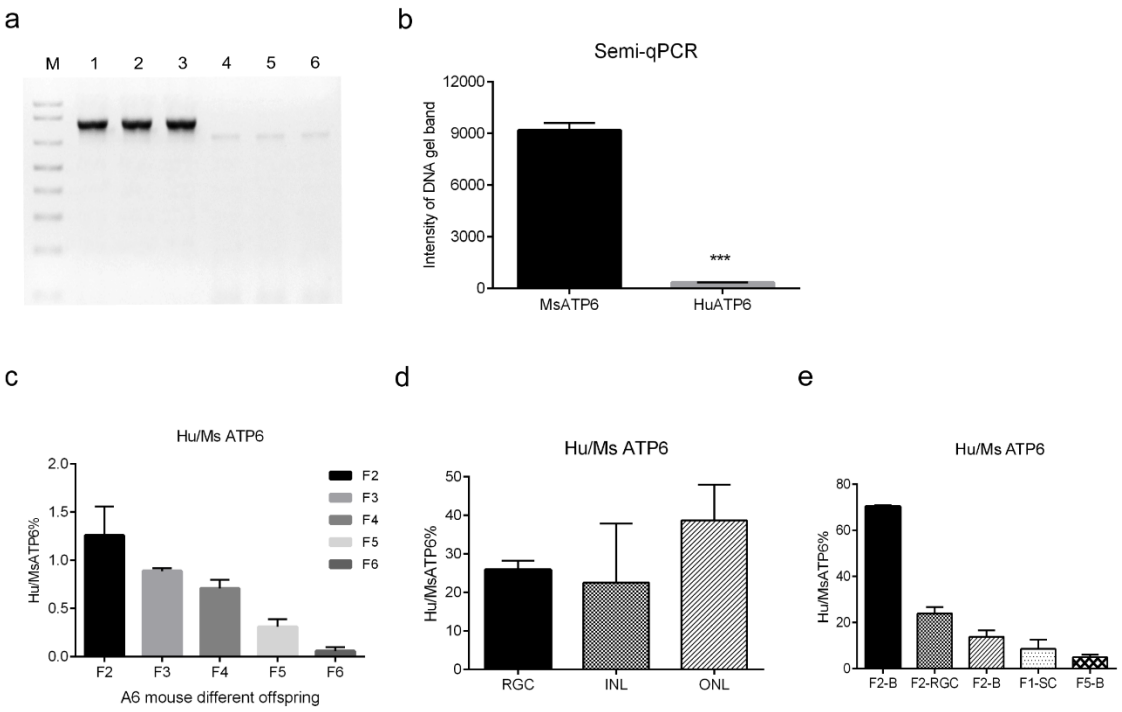

Figure 3 Heteroplasmy of ATP6 allele in A6 transgenic mice.

a. Agarose gel electrophoresis of mutant human ATP6 (lane 4, 5 and 6) and wild type mouse endogenous ATP6 (lane 1, 2 and 3) from A6 transgenic founder liver mitochondria.

b. The band intensities from PCR products as measured by Image Jshow ratios of mutant ATP6 to mouse endogenous ATP6 ~ 2.6%.

c. Ratios of mutant human ATP6 to mouse endogenous ATP6 in A6 mouse brains from F2 to F6 by qRT-PCR (n=17).

d. Quantitative PCR following laser capture microdissection showing the ratios of mutant human ATP6 to mouse ATP6 of the RGC, INL and ONL (n=2)

e. Ratios of mutant human ATP6 to mouse endogenous ATP6 in A6 mouse tissues by LCM-qPCR.

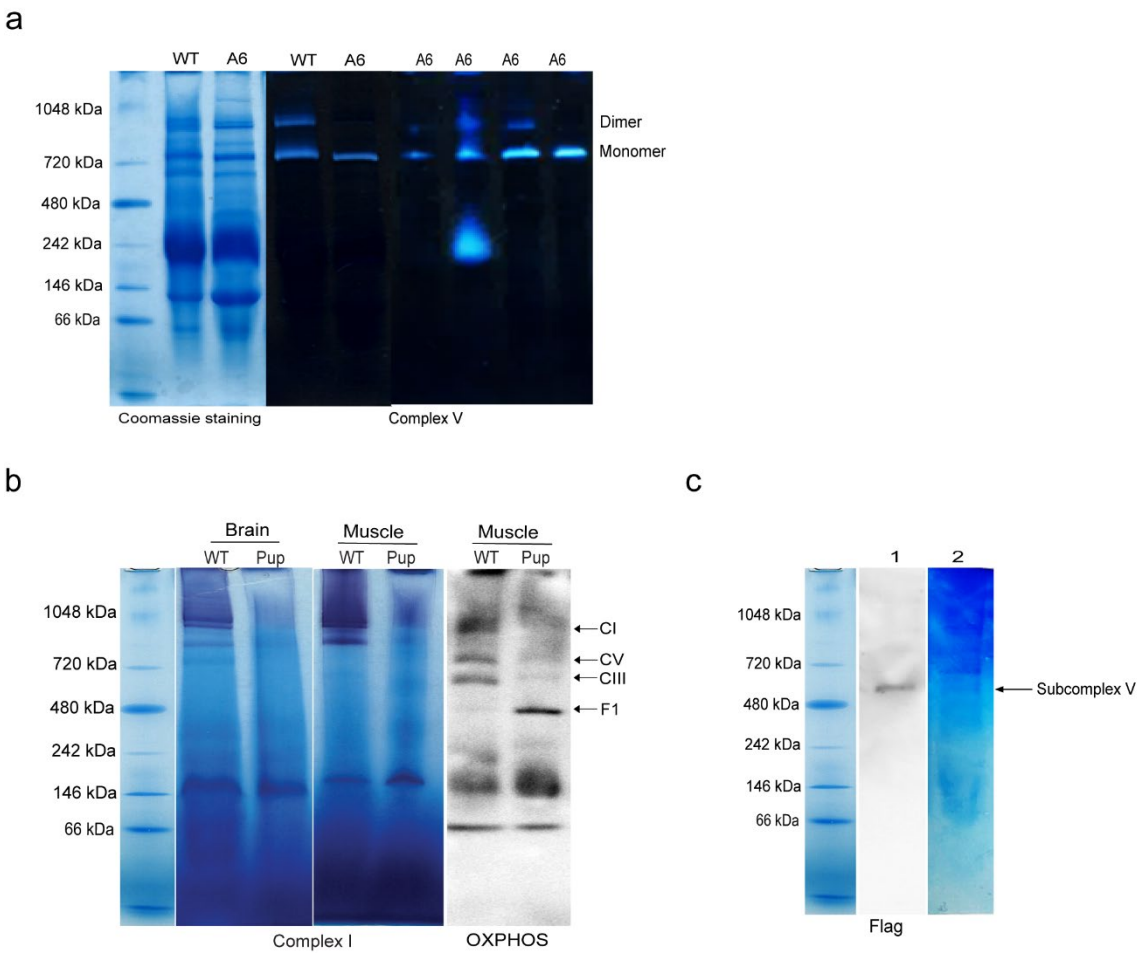

Figure 4. A6 mouse Complex V and/or Complex I in gel activity and MS sequencing.

a. Complex V in gel activity assay reveals loss of the dimer band in A6 premature death pup mouse brain compared with the wild type (left panel) and diminished dimer band intensity of A6 mouse brain, spinal cord or skeletal muscle (right panel).

b. Complex I in gel activity assay shows markedly reduced band intensities in brain and muscle samples from an F1 early death A6 pup compared to the equivalent bands from wild type mice. Western blot analyses further confirm markedly decreased staining with an OXPHOS antibody of complex I and complex V bands (left panel).

c. One dimensional native blue western blot of A6 mouse brain mitochondria shows staining with FLAG antibody (lane 1) and matched band used for MS sequencing (lane 2).

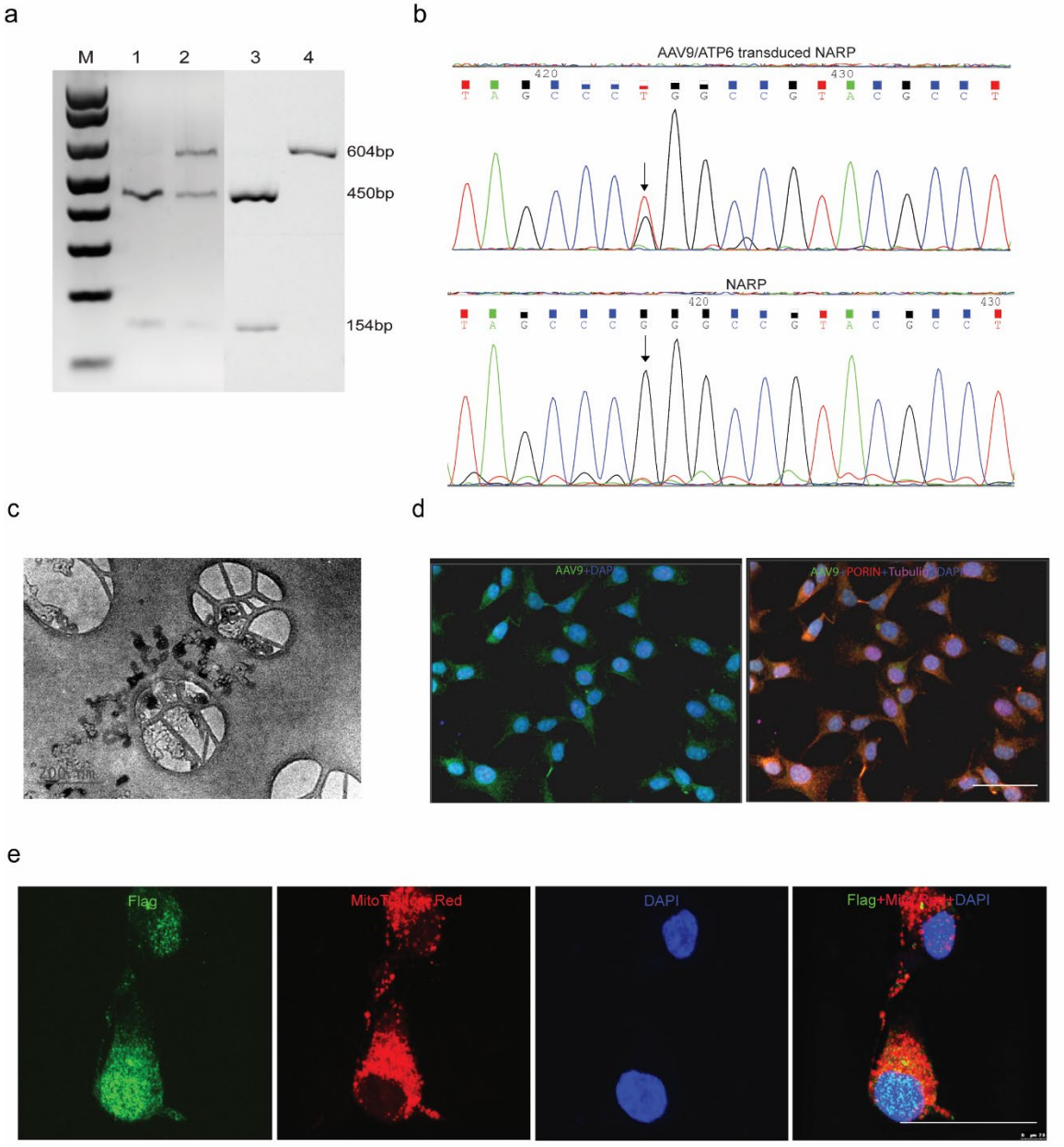

Figure 5. ATP6 expression in Hela cells and cybrids transduced with mito-targeted AAV9

a. Agarose gel electrophoresis showing that DNA fragments from uninfected homoplasmic m.8993T>G cybrid mitochondria amplified with human ATP6 primers are completely digested by Sma I (lane 1). In contrast, DNA fragments amplified from mitochondria of homoplasmic m.8993T>G cybrids infected with mito-targeted AAV9 containing wild-type *ATP6* that lacks a Sma I site were incompletely digested by Sma I (lane 2). Gel purification of the undigested band of lane 2 was completely digested by BstN1 (lane 3), but not by Sma I (lane 4) confirming wild-type human *ATP6*.

b. ABI chromatograms of DNA fragments amplified from mito-targeted AAV9-ATP6 transduced cybrids show heteroplasmy of mutant and wild-type human *ATP6* alleles (upper panel arrow). DNA fragments amplified from uninfected homoplasmic m.8993 T>G mutant cybrid cells show only the mutant allele (bottom panel arrow)**.**

c. TEM of cybrids grown on gold mesh grids and examined without counterstaining 2 hours after infection with mito-targeted AAV9 reveals viral particles within mitochondrial cristae detected by mCherry antibody.

d. Confocal microscopy of Hela cells 4h after transduction with mito-targeted AAV9; AAV detected by AAV antibody colocalized with mitochondrial marker Porin (supplementary Videos 5&6).

e. Immunofluorescence images of homoplasmic m.8993T>G cybrids transduced with AAV9 containing wild-type ATP6FLAG without cox8 targeting signal showed ATP6FLAG expression confined to the nucleus.

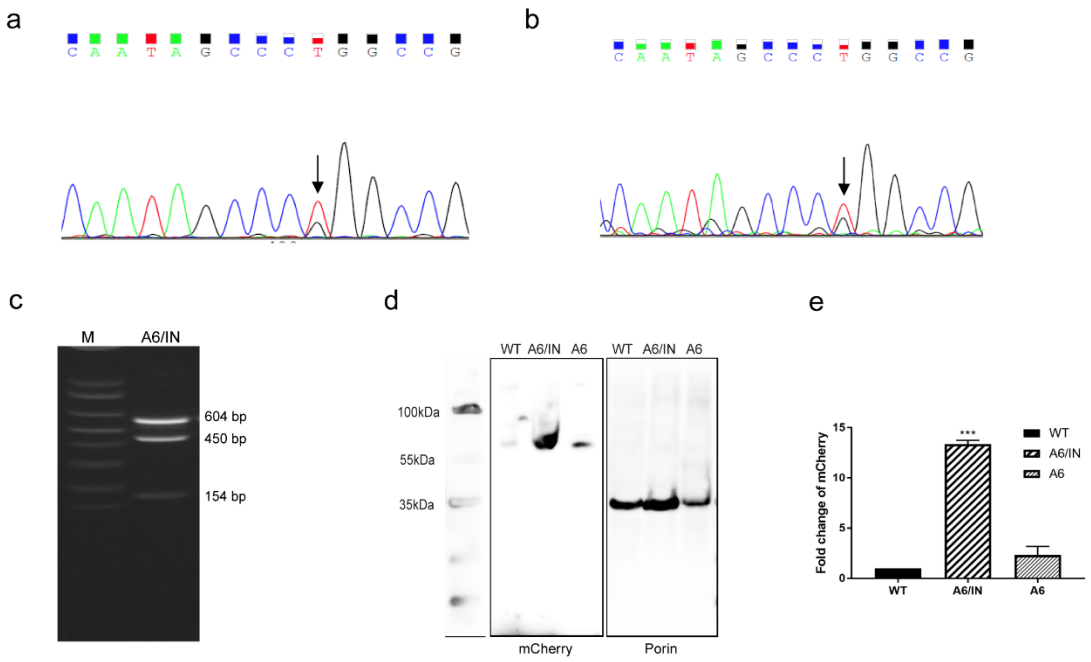

Figure 6 Wild type ATP6 expression and heteroplasmy analysis in rescued A6 mice. a-b. Sanger sequencing chromatogram of the PCR amplification products obtained from treated A6 mouse brain mitochondrial DNA shows heteroplasmy of the mutant and wild-type human ATP6 alleles (n=3, arrow). **c**. PCR amplified DNA samples from treated and untreated A6 mouse brain mitochondria were digested with Sma I and separated on 1% agarose for intensity quantification using image J and the percentage ratio of the T8993G mutation and wild type fragments (mutant load) calculated. The ratio of wild type to mutant was close to 50% in AAV9 rescued A6 mice. **d.** Anti-mCherry immunoblots of liver mitochondria extracts from rescued versus non-rescued A6 mice show higher mCherry signal intensity in samples from the treatment group (A6/IN) relative to untreated mice. **e**. Quantification of western blot analyses shows significantly higher mCherry expression in rescued A6 mice compared to untreated A6 mice (n=3, ***p<0.001).

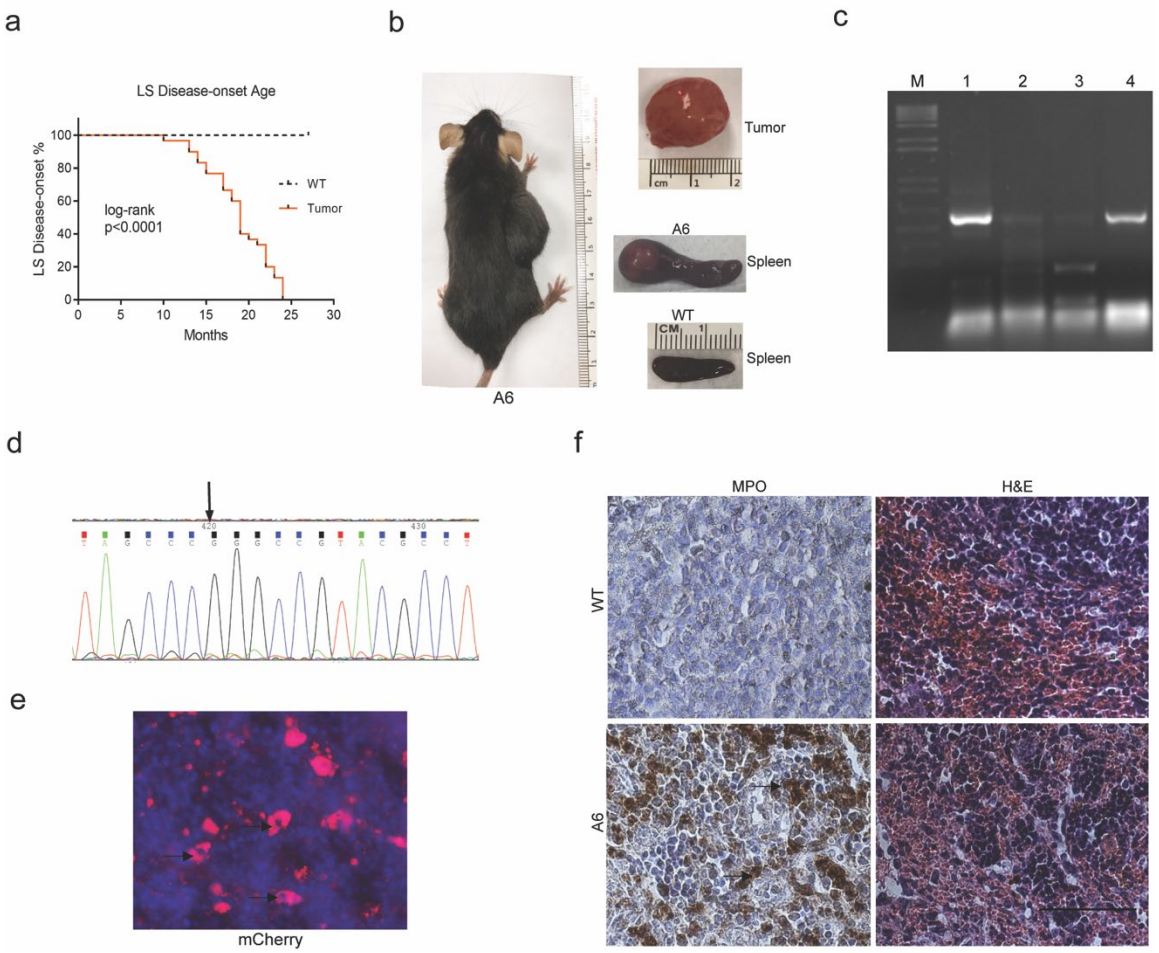

Figure 7 Tumorigenesis in a mouse model of LS/NARP induced by human m.8993 T>G mutation.

a. Cumulative proportional A6 mice with tumor onset age from 10 to 25 months (8% of A6 mice developed tumors and generations ranged from F0 to F5 A6 mice).

b. An A6 mouse with subcutaneous tumor (left panel) and tumors generated in A6 mouse spleen (right panel).

c. DNA agarose gel of mutant human ATP6 gene amplified from A6 mouse tumor mitochondria DNA mitochondria with specific human ATP6 primers.

d. ABI chromatogram of DNA fragments amplified from A6 mouse tumor shows mutant human m.8993 T>G ATP6 (arrow) containing a Sma I site (CCC/GGG).

e. Immunofluorescence image reveals endogenous mCherry expressesed in A6 mouse tumor (left panel).

f. Immunohistochemical staining for myeloperoxidase, a myeloid sarcoma marker is positive in A6 mouse spleen but not wild type (arrow, left panel, scale bar:25μm). H&E staining in A6 mouse spleen shows presence of massive malignant cells (right panel, scale bar:25μm)